Concentric Winding BLDC Motor Design

Weimin Wang, Kwanghee Nam, and Sung-young Kim
Department of Electrical Engineering, POSTECH University
Hyoja San-31, Pohang, 790-784 Republic of Korea
Tel:(82)54-279-2218, Fax:(82)54-279-5699,
Email: eewangwm@postech.ac.kr

Abstract— **Concentric winding method is preferred for low cost permanent magnet(PM) motors applicable to home appliances. The MMF of the concentric winding looks like a square function so that it has severe space harmonics. To minimize the torque ripple, special effort needs to be applied to reduce the rotor field harmonics, since they make EMF harmonics in conjunction with the MMF harmonics. In this work, the relation between EMF harmonics and rotor field harmonics is derived for a given rectangular winding function. Also, as a means to reduce the harmonics, arc shaped air gap bridge is added on the top surface of the rotor magnet. FEM simulations were repeated by changing the arc radius. In choosing the optimal one, average air gap field density B_{ave}, as well as the field harmonic is considered.**

I. Introduction

The BLDC motors were mainly used for industrial applications due to its relative high manufacturing cost. With the reduction of permanent magnet cost, application of BLDC motor is spreading even to home appliances such as air conditioner, refrigerator, washing machine, etc. The major reason that home appliance makers are trying to use BLDC motors lies on its high efficiency. Specifically, the efficiency of small induction motor is around 75%, whereas the efficiency of BLDC motor is around 90%. However, since the cost of BLDC motor is higher than the competing existing solutions, its market share is still low. Means of reducing the cost are pursued in permanent magnet, winding method, and BLDC motor drive.

Recently, concentric winding BLDC motors has been developed a lot. Concentric winding motors are very advantageous in setting up automatic production line. With the use of concentric winding, coil insertion machine can be eliminated, and thereby winding and insertion processes become extremely simple. On the other hand, the great disadvantage of concentric winding is that it has huge amount of space harmonics. When the stator has concentric pole/winding, its corresponding MMF look like a rectangular function. However, according to the orthogonal property between stator and rotor harmonics, if there is no harmonics in the rotor field, the space harmonic of stator is not a problem.

In suppressing the pulsating torque, there are two approaches: one by controlling the stator current and the other by improving the motor design. For the second approach, the effects of skew, pole count, slot count, stator ampere-turns, rotor magnetization, stator conductor distribution, magnet magnetization, and stator material processing have been considered [1]-[3]. Shape modification have been used to minimize back-EMF harmonics [4]-[5]. Some optimization technique and CAD software based analysis algorithms were used [6],[7], but these algorithms depend on an approximation of air gap flux-density distribution. Demerdash and Nehl[8] and Hanselman[9] utilized piecewise linear curves in generating back-EMF. But this approach is too complicated to deal with multiple harmonic distribution at the same time.

In this work, based on Fourier analysis we find analytically the relation between EMF harmonics and rotor field harmonics for a given rectangular winding function. Also, we derive a relation between the torque ripple and EMF harmonics. Finally, we add extra air gap bridge on the top of the magnet in order to control harmonics. FEM simulations were performed for several cases.

II. Back-EMF waveform calculation

Fig. 1 shows the cross sectional view of the 4 pole - 6 slot motor studied in this work. Since it has a single tooth per phase, in the Fig. 2, the phase winding function $N(\theta)$ look a square wave. We denote by W_s be the tooth width and by τ pole pitch. Let $\delta = W_s/(2\tau/3)$. Then δ denotes the tooth pitch factor. Note that $N(\theta)$ is not symmetrical with respect to the horizontal axis. Specifically, the magnitude of the positive side is two times larger than that of the negative side, whereas the negative interval (240 electrical degree) is two times larger than the positive interval (120 electrical degree). Expressing $N(\theta)$ as Fourier series, we obtain

$$N(\theta) = \sum_{k=-\infty}^{\infty} N_k e^{jk\theta}, \quad (1)$$

0-7803-8987-5/05/$20.00 ©2005 IEEE.

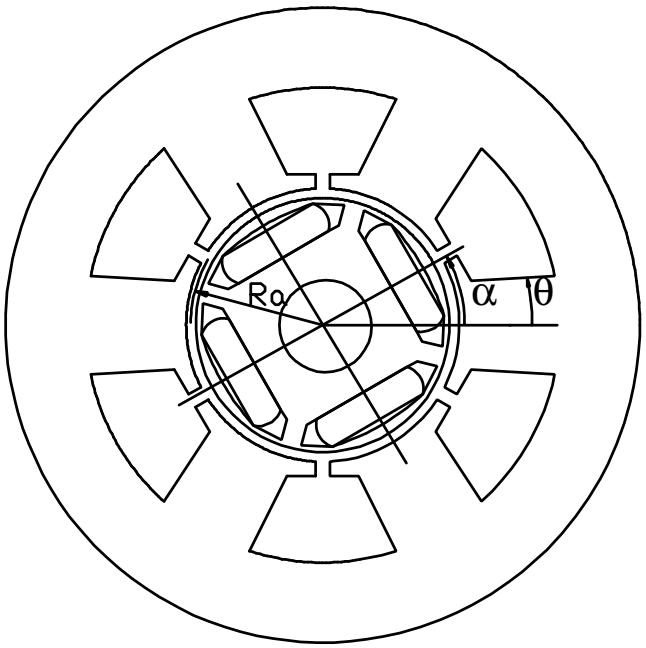

Fig. 1. Cross sectional view of a 4-pole 6-slot PM motor with concentric winding

$$N_k = \frac{1}{2\pi}\int_{-\pi}^{\pi} N(\theta)e^{-jk\theta}d\theta \quad (2)$$

$$= \frac{1}{k\pi}\sin(\frac{\delta k\pi}{3})[1-\cos(k\pi)\cos(\frac{k\pi}{3})]\,. \quad (3)$$

We denote by $B_r(\theta-\alpha)$ the radial rotor flux generated by permanent magnet, where α is the displaced angle. Then, the flux linkage with the stator winding is given by

$$\lambda(\alpha) = \int_{-L/2}^{L/2}\int_{-\pi}^{\pi} PN(\theta)B_r(\theta-\alpha)R_a d\theta dz \quad (4)$$

where P is number of pole pairs, R_a is the mean radius of the air gap and L is the effective stack length. The rotor flux density is also expressed by Fourier series such that

$$B_r(\theta-\alpha) = \sum_{n=-\infty}^{\infty} B_{rn}e^{jn(\theta-\alpha)}\,. \quad (5)$$

Substituting (1) and (5) into (4) we obtain

$$\lambda(\alpha) = \sum_{n=-\infty}^{\infty}\lambda_n e^{jn\alpha} \quad (6)$$

$$\lambda_n = PR_aLB_{rn}\int_{-\pi}^{\pi}\sum_{k=-\infty}^{\infty} N_k e^{-j(n-k)\theta}d\theta \quad (7)$$

$$= 2PR_aLB_{rn}\left(\sum_{k\neq n} N_k\frac{\sin\left[(n-k)\pi\right]}{n-k} + N_k\pi\right) \quad (8)$$

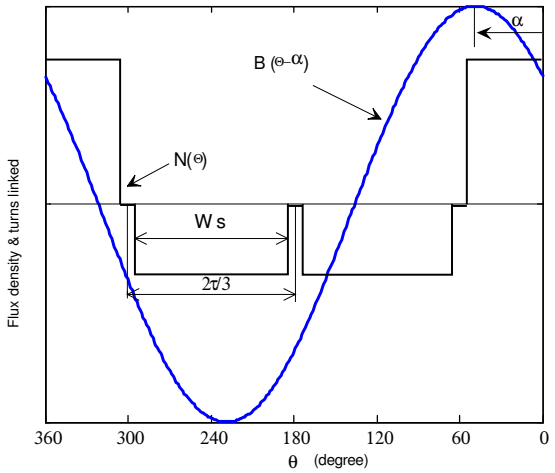

Fig. 2. Rectangular shape MMF N caused by concentric winding design and rotor flux density function B_r.

Note that the back-EMF is given by $e = -\frac{d\lambda}{dt} = -\frac{\partial\lambda}{\partial\alpha}\frac{d\alpha}{dt}$. Letting $\omega = \frac{d\alpha}{dt}$, we obtain from (6), (8) and (3)that

$$e(\alpha) = \sum_{n=-\infty}^{\infty} E_n e^{jn\alpha} \quad (9)$$

$$E_n = -jn\omega\lambda_n = j\gamma_n B_{rn}, \quad (10)$$

where

$$\gamma_n = -2\omega nPR_aL\sin(\frac{\delta n\pi}{3})[1-\cos(n\pi)\cos(\frac{n\pi}{3})] \quad (11)$$

$$= \begin{cases} 0, & n = 3k \\ -3\omega PR_aL\sin(\frac{\delta n\pi}{3}), & n \neq 3k \end{cases} \quad (12)$$

Note that E_n is the EMF n^{th} harmonic caused by the n^{th} harmonic B_{rn} of the rotor field. Therefore, $\gamma_n = Im\{E_n\}/B_{rn}$ is the natural EMF's sensitivity function with respect to the rotor field harmonics. Fig. 3 shows the γ_n versus δ for each harmonic. From Fig. 3, we can observe that we may reduce EMF harmonic by decreasing tooth pitch factor δ and adjust the relative strength among harmonics by selecting proper δ. A proper range of δ is (0.85,0.95).

III. EMF Harmonic Sensitivity Analysis

It is easy to see from (10) that a prefect sinusoidal flux density distribution does not generate EMF harmonics. The n^{th} harmonic B_{rn} of the rotor field produces only n^{th} harmonic E_n of EMF. Thus, the effects of field harmonic on the EMF harmonic can be seen by γ_n. Note that γ_n is not dependent on the shape of the rotor field. It is totally determined by the shape of winding function $N(\theta)$. It is easy to find from

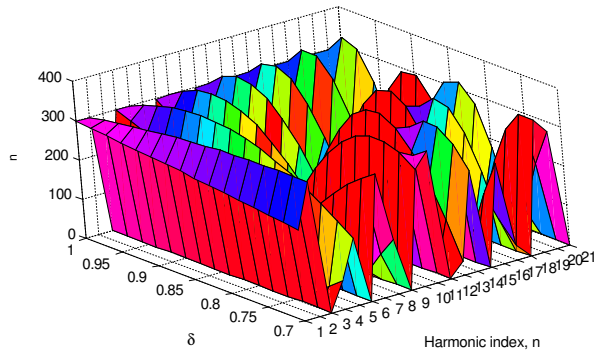

Fig. 3. Coefficient $|\gamma_n|$ versus tooth pitch factor δ and harmonic indices

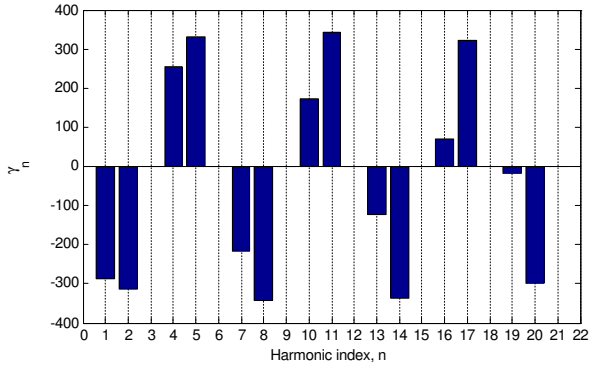

Fig. 4. γ_n for different harmonic indices when $\delta = 0.95$

(12) that the multiples of third harmonics (3,6,9,12,15,18,21..) field do not induce any back-EMF harmonics. The calculation results are shown in Fig. 4 with $\delta = 0.95$. Note that γ_n for $n = 3k+2$ (2,5,8,11,14,17,20) are big, and they do not decay as the index increases. On the other hand, γ_n for $n = 3k+1$ (4,7,10,13,16,19) decay rapidly. as the index increases. Hence, special care needs to be paid not to excite $n = 3k+2$ harmonics in developing low torque ripple machines.

IV. Rotor Air Gap Bridge Design Based on FEM Analysis

The basic rotor core is shown in Fig.5. The PM which has flat surfaces on the top and bottom is inserted in the rotor core. On both sides of the PM, air gap bridge are provided to prevent flux short. In this design, additional air gap bridge is added on the top of PM. The air gap bridge has an arc shape. The basic rationale for such arc shape is to defocus the field on the direct (d) axis. Then, the air gap field density will tends to have an arc shape on the top, instead of flat plateau shape. In other words, the global air gap field shape will be closer to the sinusoidal one.

However, the sacrifice is the reduction of the field average B_{ave}. In order to see the both harmonic content and field average , we define harmonic coefficients β and B_{ave} as follows:

$$B_{ave} = \frac{\int_0^{2P\pi} |B_r| d\xi}{2P\pi}, \tag{13}$$

$$\beta = \frac{\sqrt{\sum_{k=2}^{12} B_{rk}^2}}{|B_{r1}|}. \tag{14}$$

Note that β implies the ratio of power of harmonics to 12 to the fundamental component.

The design control point is the radius of the arc denoted by ρ. The arc starts from a top edge of PM to the other top edge. By controlling the magnitude of ρ, the area of the air gap bridge is changed. Eleven simulations were done with the motor parameters shown in Table I for $\rho = 12.9,\ 13.8,\ 14.6,\ 15.5,\ 17.3,\ 25.7,\ 34.4,\ 43.2,\ 52.1,\ 56.6,\ 61$(mm). Fig. 5 shows only 3 cases where

$$\begin{aligned} &(a) \quad \rho(12.9\text{mm}) < R(18\text{mm}) \\ &(b) \quad \rho(17.3\text{mm}) \simeq R(18\text{mm}) \\ &(c) \quad \rho(61\ \text{mm}) > R(18\text{mm}). \end{aligned}$$

The middle row of Fig. 5 shows the flux lines and the third row shows the air-gap flux densities.

Fig. 6 shows B_{ave} versus ρ and Fig. 7 shows β versus ρ. Harmonic increases as the bridge area gets smaller, i.e., harmonic content is the greatest when there is no air gap bridge. Hence for less harmonic, it is better to decrease ρ with the increase of the air gap area. However, as ρ decreases, B_{ave} also decreases as shown in Fig. 6. Decrease in B_{ave} implies smaller torque. To consider such trade-off, we define a new performance index η such that

$$\eta = \frac{B_{ave}}{\beta}. \tag{15}$$

Performance index η implies the field average per harmonic coefficient. Fig. 8 displays η versus ρ. η is maximized at $\rho = 52mm$. At this time, the maximum height of the air gap bridge is 0.52mm.

V. Concluding Remarks

In the first part, the harmonic coefficients of EMF were calculated when the MMF function has a rectangular shape which is common to concentric winding motors. The result tells us that even with the rectangular shape MMF, the EMF function can be sinusoidal if there is no harmonics in rotor field. The coefficients γ_n relating EMF harmonic to rotor field

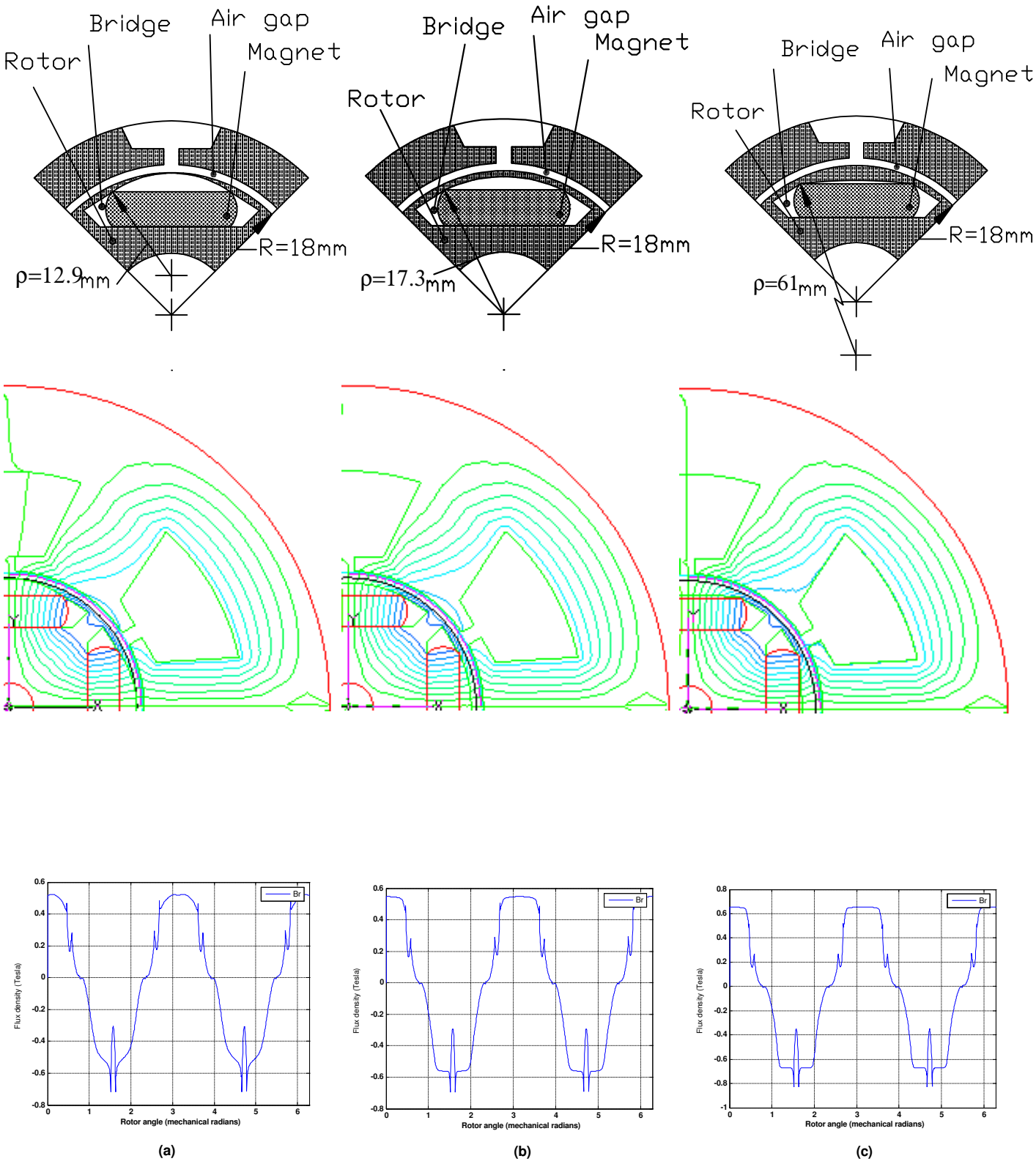

Fig. 5. Rotor shapes with air gap bridge (first row), FEM simulation results (second row), air gap field density and for three different air gap bridge arc radii: (a)$\rho = 12.9$mm, (b)$\rho = 17.3$mm, and (c)$\rho = 61$mm.

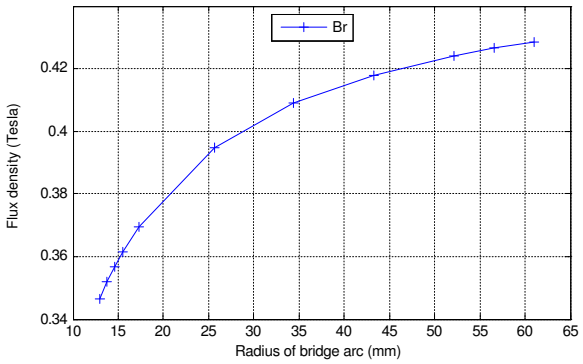

Fig. 6. Average air gap field density B_{ave} versus different air gap bridge arc radii ρ.

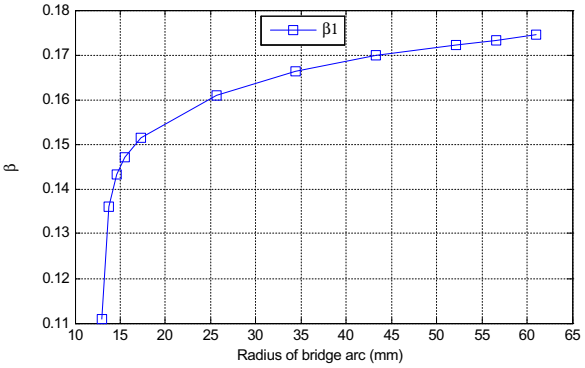

Fig. 7. Harmonic coefficient β versus different air gap bridge arc radii ρ.

harmonic were strong at $n = 3k + 2$. In the second part, rotor was designed with the air gap bridge on the top of PM. With the increase of the air gap bridge area, harmonic is decreasing. But, the average field decreases when the area increases. An optimal value was found for an example. This method could be used to modify PM magnet motor design when improvement is necessary in harmonics.

REFERENCES

[1] D.C.Hanselman, "Effect of skew, pole count and slot count on brushless motor radial force, cogging torque and back EMF," *Electric Power Applications, IEE Proceedings-,Vol.144*, pp. 325-330, Sept. 1997.

[2] S.Murthy, B.Derouane,B.Liu and T.Sebastian, "Minimization of torque pulsations in a trapezoidal back-EMF permanent magnet brushless DC motor," *Industry Applications Conference, Vol.2*, pp. 1237-1242, Oct. 1999.

[3] T.Sebastian and V.Gangla, "Analysis of induced EMF waveforms and torque ripple in a brushless permanent magnet machine," *IEEE Trans. Ind. Applicat.Vol. 32*, pp. 195-200, Jan./Feb.1996.

[4] J.H.Lee, D.H.Kim and I.H.Park, "Minimization of higher back-EMF harmonics in permanent magnet motor using shape design sensitivity with B-spline parameterization," *IEEE Trans.Magn.,Vol. 39* , pp. 1269-1272, May. 2003.

[5] Y.Perriard,C.Koechli and L.Cardoletti, "Noise reduction for brushless DC motor-sensorless control analysis and back-EMF shape modification," *IECON 02 vol.2*, pp. 1038-1043, Nov. 2002.

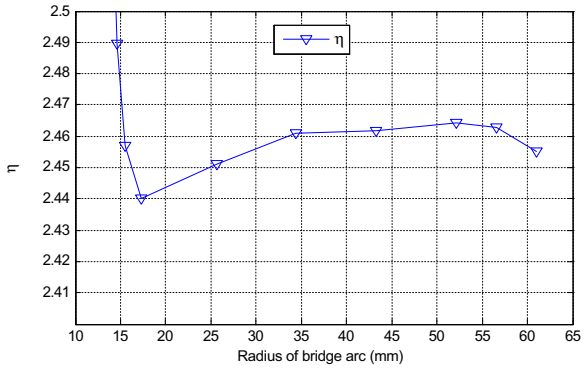

Fig. 8. Performance index $\eta(\equiv B_{ave}/\beta)$ versus different air gap bridge arc radii ρ.

TABLE I
SIMULATED MOTOR DATA

Number of phases	3
Number of stator slots	3
Number of magnet poles	2
Slots/Pole/phase	0.5
Stack length	100mm
Rotor outer diameter	36mm
Air gap length	1mm
Magnet thickness	4mm
Turns/phase	80
Magnet magnetization	Radial

[6] Y.Fujishima, S.Wakao, M.Kondo and N.Terauchi, "An optimal design of interior permanent magnet synchronous motor for the next generation commuter train," *IEEE Trans.Applied Superconductivity*, pp. 1902-1905, June 2004.

[7] T.J.E.Miller and R.Rabinovici, "ABack-EMF waveforms and core losses in brushless DC motors," *Electric Power Applications, IEE Proceedings-Vol.141*, pp. 144-154, May. 1994.

[8] N.A. Demerdash and T.W.Nehl, "Dynamic modeling of brushless dc motors for aerospace actuation," *IEEE Trans. Aerosp. Electron. Syst., vol. AES-16*, pp. 811-821, Nov.1980.

[9] D.C.Hanselman,"Brushless Permanent Magnet Motor Design," *The Writers' Collective*, Second Edition. April 2003.